# Patchwork Reconstruction with Resolution Modeling for Digital Breast Tomosynthesis

Koen Michielsen, Katrien Van Slambrouck, Anna Jerebko and Johan Nuyts

***Abstract*—Visualizing micro-calcifications adequatly remains a challenge in digital breast tomosynthesis. We propose a maximum a posteriori algorithm which uses a plane by plane updating scheme for faster convergence. The scheme enables efficient implementation of an approximate model for position dependent resolution. An observer study shows an improvement in detection of micro-calcifications compared to the filtered backprojection method currently in use.**

## I. Introduction

Early detection of breast cancers by mammography screening has been shown to improve patient outcome [1]. However, some lesions, like masses in dense breasts, remain difficult to detect due to the amount of anatomical noise [2]. A three dimensional imaging technique, like digital breast tomosynthesis (DBT), may be able to solve this problem by removing interference from overlapping dense tissue [3]. DBT provides a limited angle set of projections. These projections are usually reconstructed with filtered backprojection (FBP). However, because of the limited angular range and low dose acquisitions, reconstruction by FBP is not always optimal [4], [5], especially for small angular range [6].

Using the more accurate acquisition model of the Maximum Likelihood for Transmission (MLTR) algorithm proposed in [7] could improve reconstruction for DBT, but this algorithm (like all iterative methods) is quite slow in comparison to FBP. We try to improve the convergence speed of the algorithm by applying a grouped coordinate ascent (GCA) algorithm [8], [9], where groups of voxels are updated sequentially instead of simultaneously. By choosing the reconstruction planes parallel to the detector as these groups, we can simultaneously introduce a resolution model which is dependent on the height above the detector.

## II. Materials and Methods

### A. Patchwork Reconstruction

In the MLTR algorithm, attenuation distribution $\vec{\mu}$ is obtained by maximising log-likelihood function $L$. The log-likelihood can be written as

$$L = \sum_i y_i \ln \hat{y}_i - \hat{y}_i \tag{1}$$

with $y_i$ the measured transmission scan, $\hat{y}_i$ the estimated transmission scan and $i$ the index of the projection line. In the simplest case the acquisition process can be written as:

$$\hat{y}_i = b_i e^{-\sum_j l_{ij}\mu_j} \tag{2}$$

with $b_i$ the blank value for projection line $i$ and $l_{ij}$ the intersection lenght between projection line $i$ and voxel $j$. With this information, one can construct a gradient ascent algorithm, with following update step:

$$\mu_j^{\text{new}} = \mu_j^{\text{old}} + \frac{\alpha_j \sum_i l_{ij}(y_i - \hat{y}_i)}{\sum_i l_{ij}\hat{y}_i \sum_h \alpha_h l_{ih}} \tag{3}$$

Choosing $\alpha_j = 1$ in equation 3 results in the MLTR algorithm and $\alpha_j = \mu_j^{\text{old}} + \epsilon$, with $\epsilon$ a small positive constant to make sure $\alpha_j > 0$, gives the convex algorithm [10].

For a patchwork reconstruction, the image is divided into regions (patches) that are updated separately and sequentially [11]. Accelerated convergence is partly due to the sequential updates but mainly due to an increased step size in the update. In equation 3 we can consider a patch update as an update with $\alpha_j = 0$ everywhere except in the current patch. Therefore the sum $\sum_h \alpha_h l_{ih}$ in the denominator will be smaller and the step size for updates will be larger for smaller patches. We choose to use each plane (parallel to the detector surface) in the reconstruction volume as a separate patch. This is both the logical choice, since this is how tomosynthesis images are visualized, and close to optimal, since it minimises the denominator in equation 3, indicating that voxels in one plane share little information in the projection.

Because of the limited angular sampling, there is little to no information on the distribution of attenuation values in the direction perpendicular to the detector surface. The patchwork algorithm tends to accumulate all low frequency information in the first patch. To ensure that low frequency information will be uniformily distributed over all patches, we initialize the reconstruction volume with a rough estimate of the attenuation and divide the update step for each patch in the first two iterations by the number of patches that still need to be updated in the current iteration. Because this creates a non-uniform noise distribution in the volume, the update order of the patches is reversed in the second iteration.

### B. Resolution Modeling

While the detectors in mammography tomosynthesis systems have good resolution, tube motion during the acquisition causes additional blurring in the acquisition of tomosynthesis data. Mathematically this blurring can be added to the simple aqcuisition model in equation 2 as follows:

$$\hat{y}_i = b_i \sum_n A_{in} \int_{\theta_1}^{\theta_2} w(\theta) e^{-\sum_j l_{nj}(\theta)\mu_j} d\theta + s_i \tag{4}$$

K. Michielsen, K. Van Slambrouck and J. Nuyts are with the department of Nuclear Medicine, KU Leuven, Belgium

A. Jerebko is with Siemens AG, Erlangen, Germany

This work is supported by Siemens AG and by SBO project QUANTIVIAM (060819) of the Institute for Promotion of Innovation through Science and Technology in Flanders (IWT-Vlaanderen).

Corresponding author: koen.michielsen@uzleuven.be

With the angles $\theta$ representing the tube motion during one of the acquisitions of the tomosynthesis series, $w(\theta)$ is the relative weight of each angle within a single exposure. The scatter is represented by $s_i$, and the kernel with coefficients $A_{in}$ represents the intrinsic detector blurring.

Although equation 4 describes the acquisition process adequatly, the derived update step would be too complex for an efficient reconstruction. Therefore we introduce the following approximation, making use of the fact that the volume is already split in patches parallel to the detector plane:

$$\hat{y}_i = b_i \prod_p \sum_n A_{in}^p e^{-\sum_{j\in p} l_{nj}\mu_j} + s_i \tag{5}$$

In essence, the motion blur, which is dependent on the height above the detector plane, is included in the detector blur $A_{in}^p$ for each patch $p$.

Using the following notation, we can derive the update step for an MLTR algorithm using this model for the acquisition.

$$\hat{y}_i = b_i \prod_p \bar{\psi}_i^p + s_i \tag{6}$$

$$\bar{\psi}_i^p = \sum_n A_{in}^p \psi_n^p \tag{7}$$

$$\psi_i^p = e^{-\sum_{j\in p} l_{ij}\mu_j} \tag{8}$$

The patches appear in equation 8 in the form of the sum over $j$: $\sum_{j\in p} l_{ij}\mu_j = \sum_j \alpha_j l_{ij}\mu_j$ with $\alpha_j = 1$ for $j \in p$ and $\alpha_j = 0$ for $j \notin p$. With this we can calculate the update step in eq. 9.

$$\Delta\mu_j = \frac{-\frac{\partial L}{\partial \mu_j}}{\sum_k \frac{\partial^2 L}{\partial \mu_j \partial \mu_k}} \tag{9}$$

$$-\frac{\partial L}{\partial \mu_j} = \sum_i l_{ij}\psi_i^{p(j)} \sum_n A_{in}^{p(j)} \frac{y_n - \hat{y}_n}{\bar{\psi}_n^{p(j)}} \frac{\hat{y}_n - s_n}{\hat{y}_n} \tag{10}$$

$$\sum_k \frac{\partial^2 L}{\partial \mu_j \partial \mu_k} \approx -\sum_i l_{ij}\psi_i^{p(j)} \cdot \sum_k l_{ik} \cdot \sum_n A_{in}^{p(j)} \frac{\hat{y}_n - s_n}{\bar{\psi}_n^{p(j)}} \left(1 - \frac{y_n s_n}{\hat{y}_n^2}\right) \tag{11}$$

The approximation for the second derivative comes from the assumption that the intersection lengths are smooth on the scale of the kernel $A_{in}^p$:

$$\sum_n A_{in}^p \psi_n^p \sum_{k\in p} l_{nk} \approx \sum_{k\in p} l_{ik} \sum_n A_{in}^p \psi_n^p \tag{12}$$

### C. Phantom Simulation and Reconstruction

To test the reconstruction method, we simulated background images with stochastical noise by filtering white noise with a power law filter $f(\nu) = \kappa/\nu^\beta$, with $\nu$ the frequency, $\beta = 3$ and $\kappa = 10^{-5}$ mm$^{-1}$ [12], [13]. The resulting images were reduced to 500 by 500 by 200 isotropic voxels with sides of 85 $\mu$m. This background volume was placed in one of three possible locations, always with one side above the chest-side detector edge: central at 27 mm above the detector plane, central at 67 mm above the detector plane, and 75 mm off center at a height of 47 mm.

We used the background images to generate two data sets: in the first set we added a random number of clusters to each background image, Poisson distributed with a mean of 1.0 per image, and placed at a random location within the volume (but not on the edge). Each cluster consisted of a random number of calcifications, with a mean of 2.5 per cluster (again Poisson distributed), but with a minimum of a single calcification per cluster. The individual calcifications were spherical, with a diameter between 100 and 200 $\mu$m, spaced 0.5 to 1.5 mm apart in a random direction and set in a volume with isotropic voxel spacing of 5 $\mu$m.

For the second set we created two series of micro-calcifications (smooth, corresponding to Le Gal II and irregular, corresponding to Le Gal IV) according to the recipe of Näppi [14]. These micro-calcifications were rescaled to diameters between 200 and 600 $\mu$m. The volume in which they were set had isotropic voxel spacing between 6 and 18 $\mu$m, depending on the rescaling.

Projections of these volumes were simulated according to the acquisition model described in eq. 4 and with increased detector sampling. Multiple source positions were sampled for each exposure angle, corresponding to an exposure time of 120 ms per projection, x-ray energy was set to 20 keV and Poisson noise was generated with a blank scan of 1500 photons per pixel (12.5 $\mu$Gy detector dose after attenuation).

The geometric blurring parameters for our model were determined for the Mammomat Inspiration[1] system (Siemens, Erlangen, Germany), which is in clinical use on site. Therefore the Siemens iFBP method [15] without detector binning, with slice thickness filter and with a filter designed so that resulting reconstructed slices resemble 2D mammography images was used as the point of reference. The two reconstructions to be compared to the point of reference were 3 iterations of our patchwork reconstruction with resolution modelling, with prior and without prior. The Huber prior (equation 13) was used, with $\beta = 3.0 \cdot 10^{-4}$ and $\delta = 2.5 \cdot 10^{-4}$ mm$^{-1}$. Since the average reconstructed attenuation is about 0.06 mm$^{-1}$, the prior function is mostly active in linear mode.

$$\begin{aligned} |\mu_j - \mu_k| < \delta: \;\; P(\vec{\mu}) &= \sum_{j,k} w_{jk} \frac{(\mu_j - \mu_k)^2}{2\delta^2} \\ |\mu_j - \mu_k| \geq \delta: \;\; P(\vec{\mu}) &= \sum_{j,k} w_{jk} \frac{|\mu_j - \mu_k| - \delta/2}{\delta} \end{aligned} \tag{13}$$

Figure 1 shows an example of the three reconstruction methods for two simulated calcifications.

We compare the convergence speed of the two patchwork iterative methods used in the observer study with the MLTR and Convex algorithms by plotting, $L_{max} - L$ in function of iteration number for the reconstruction of a mathematical phantom [16].

[1]Breast tomosynthesis with Siemens MAMMOMAT Inspiration is an investigational practice and is limited by U.S. law to investigational use. It is not commercially available in the U.S. and its future availability cannot be ensured.

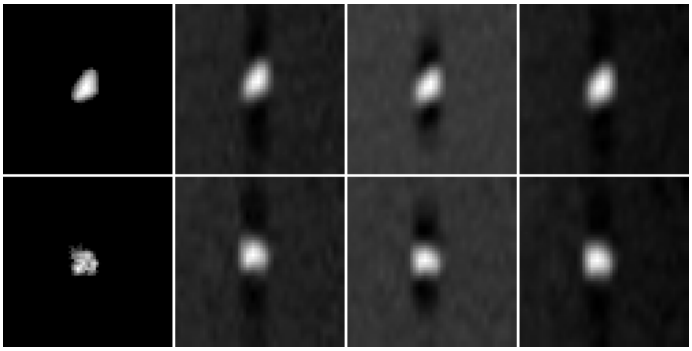

Fig. 1: Two simulated calcifications with a diameter of 400 $\mu$m. Window is set from minimum to maximum pixel value. Top: smooth, bottom: irregular; from left to right: true slice, iFPB, patchwork iterative without prior and with prior.

### D. Reconstruction Comparison

The comparison was split in two distinct observer experiments: first, a free search study to check the detectability of small spherical micro-calcifications and second, a two-alternate forced choice (2AFC) study to check the discrimination between smooth (Le Gal II) and irregular (Le Gal IV) micro-calcifications.

For the detection study, 7 readers performed a free search on 120 cases for each reconstruction (with 40 images used for initial training) and scored detected lesions on a 4 point scale as shown in table I. Results were analyzed using the weighted JAFROC method [17].

| Score | Description |
|---|---|
| 1 | I see a hint of a calcification |
| 2 | This might be a calcification |
| 3 | This is probably a calcification |
| 4 | I am sure this is a calcification |

TABLE I: Evaluation scale for the detection experiment.

For the 2AFC study, 5 readers evaluated 300 cases for each reconstruction (of which 100 cases were used as initial training) by classifying them as smooth or irregular and providing their certainty of this classification (low, medium or high certainty). Results were analysed using the DBM MRMC method [18].

## III. Results

Figure 2 shows results for the detection study. The extension from the point of the lowest confidence score (1 in table I) is shown in grey. There are significant differences between the iFBP and the patchwork reconstruction with prior (p = 0.029) and between both patchwork reconstructions (p = 0.022) for detecting the smallest micro-calcifications ($<$200 $\mu$m). There is no difference between the iFBP and the patchwork reconstruction without prior (p = 0.893).

Table II shows the results for the shape discrimination study with the area under the ROC curve (AUC) as the figure of merit (FoM). The p-value of 0.935 indicates that the three reconstruction methods have identical performance when considering shape discrimination of small lesions.

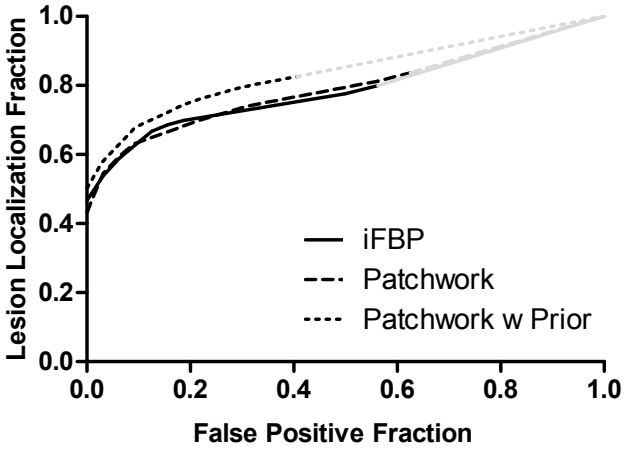


Fig. 2: AFROC curve of detection study results.

| Reconstruction | Figure of Merit |
|---|---|
| iFBP | 0.774 |
| Patchwork | 0.773 |
| Patchwork w Prior | 0.769 |
| p-value | 0.935 |

TABLE II: Results of the 2AFC study.

Figure 3 shows the likelihood as a function of the iteration number. The patchwork reconstruction with prior is not shown since its curve would overlap that of the normal patchwork reconstruction on the graph. The patchwork reconstructions reach a better likelihood value than the MLTR reconstruction at 10 and 20 iterations after only 5 and 7 iterations respectively.

## IV. Discussion

The initial evaluations show that the patchwork reconstruction with resolution modelling and smoothing prior can improve upon iFBP after only 3 iterations for detecting very small micro-calcifications while performing at the same level for classifying slightly larger micro-calcifications.

The new algorithm currently results in a limited improvement on the clinical image quality, as shown in a comparison with iFBP in figure 4. This makes sense when considering the fact that the iFBP algorithm has been specifically optimised for the Mammomat Inspiration system. We expect further

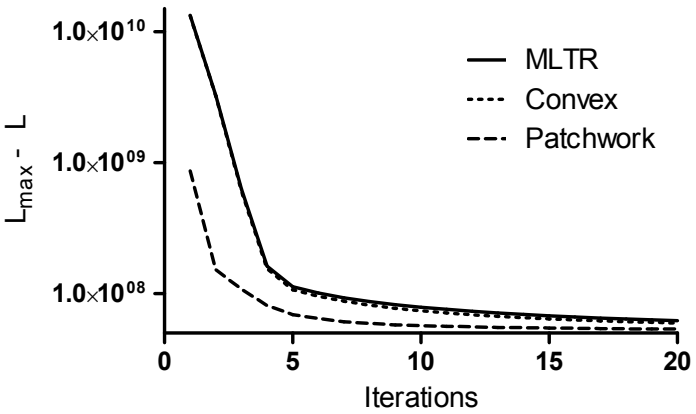


Fig. 3: Likelihood ($L_{max} - L$) curve.

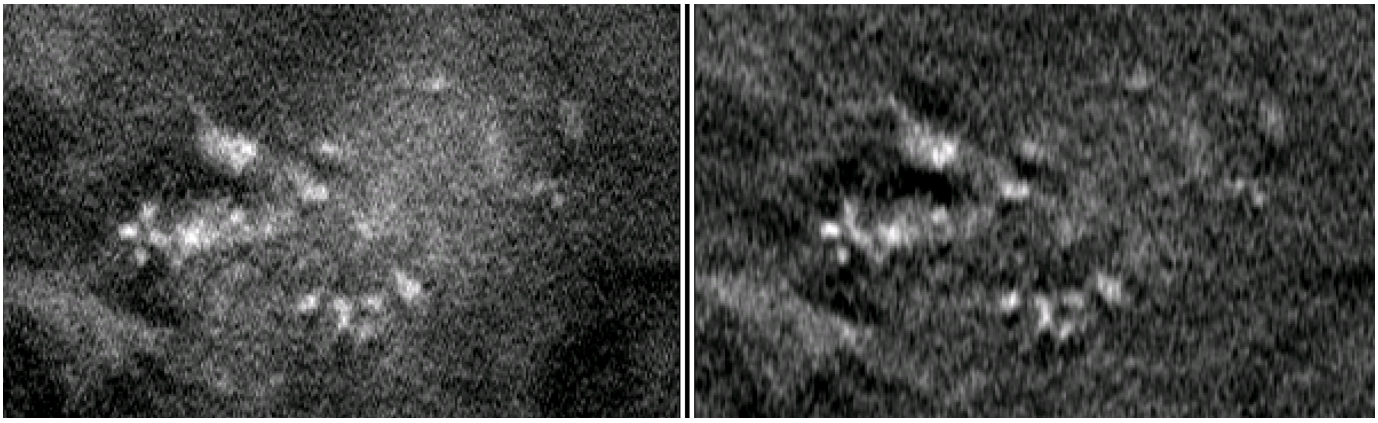

Fig. 4: A cluster of micro-calcifications (left: iFBP, right: patchwork reconstruction with resolution modelling).

improvements in our algorithm when including the measured point spread functions of the system in the resolution model instead of a Gaussian approximation.

An important advantage in comparison to other iterative methods is the improved convergence speed that comes from applying a grouped coordinate ascent algorithm. The much faster convergence speed per iteration step reduces one of the most critical factors that keeps iterative reconstruction from being used in the clinic: reconstruction time. In our results we only used 3 iterations while typically we would use 8-10 iterations without the GCA algorithm.

## V. Conclusions

The described method greatly increases convergence rate per iteration of DBT reconstruction while including an accurate resolution model. Adding a Huber-prior to the algorithm limits the noise in the image and allows reconstruction of clinical images in only 3 iterations while increasing detection performance in comparison to iFBP and maintaining the same level of lesion discrimination performance.

## Acknowledgements

The authors would like to thank Nicholas Marshall for providing the MTF measurements for the resolution model; Federica Zanca for her advice on designing the observer study; and Joke Bints, Gregory Cieters, Lesley Cockmartin, Annelies Jacobs, Xochitl Lopez Rendon, Ahmadreza Rezaei, Elena Salvagnini, Eman Shaheen and Lin Zhou for their participation in the observer study.

## References

[1] L. Nyström, I. Andersson, N. Bjurstam, J. Frisell, B. Nordenskjöld, and L. E. Rutqvist, "Long-term effects of mammography screening: updated overview of the Swedish randomised trials." *Lancet*, vol. 359, no. 9310, pp. 909–19, Mar. 2002.

[2] R. E. Bird, T. W. Wallace, and B. C. Yankaskas, "Analysis of cancers missed at screening mammography." *Radiology*, vol. 184, no. 3, pp. 613–617, Sep. 1992.

[3] J. A. Baker and J. Y. Lo, "Breast tomosynthesis: state-of-the-art and review of the literature." *Academic Radiology*, vol. 18, no. 10, pp. 1298–1310, Oct. 2011.

[4] T. Wu, R. H. Moore, E. A. Rafferty, and D. B. Kopans, "A comparison of reconstruction algorithms for breast tomosynthesis," *Medical Physics*, vol. 31, no. 9, pp. 2636–2647, 2004.

[5] Y. Zhang, H.-P. Chan, B. Sahiner, J. Wei, M. M. Goodsitt, L. M. Hadjiiski, J. Ge, and C. Zhou, "A comparative study of limited-angle cone-beam reconstruction methods for breast tomosynthesis," *Medical Physics*, vol. 33, no. 10, pp. 3781–3795, 2006.

[6] T. Mertelmeier, J. Ludwig, and B. Zhao, "Optimization of tomosynthesis acquisition parameters: angular range and number of projections," in *LNCS Proceedings of the IWDM*, J. Marti, A. Oliver, J. Freixenet, and R. Marti, Eds., 2008, pp. 220–227.

[7] J. Nuyts, B. De Man, P. Dupont, M. Defrise, P. Suetens, and L. Mortelmans, "Iterative reconstruction for helical CT: a simulation study." *Physics in Medicine and Biology*, vol. 43, no. 4, pp. 729–737, Apr. 1998.

[8] J. A. Fessler, E. P. Ficaro, N. H. Clinthorne, and K. Lange, "Grouped-coordinate ascent algorithms for penalized-likelihood transmission image reconstruction." *IEEE Transactions on Medical Imaging*, vol. 16, no. 2, pp. 166–175, Apr. 1997.

[9] J. A. Fessler and D. Kim, "Axial block coordinate descent (ABCD) algorithm for X-ray CT image reconstruction," in *Proceedings of Fully3D*, 2011, pp. 262–265.

[10] K. Lange and J. A. Fessler, "Globally convergent algorithms for maximum a posteriori transmission tomography." *IEEE Transactions on Image Processing*, vol. 4, no. 10, pp. 1430–1438, Jan. 1995.

[11] K. Van Slambrouck and J. Nuyts, "A patchwork (back)projector to accelerate artifact reduction in CT reconstruction," in *IEEE Nuclear Science Symposium Conference Record*, no. 060819. IEEE, 2010.

[12] K. G. Metheany, C. K. Abbey, N. Packard, and J. M. Boone, "Characterizing anatomical variability in breast CT images," *Medical Physics*, vol. 35, no. 10, pp. 4685–4694, 2008.

[13] E. Engstrom, I. S. Reiser, and R. M. Nishikawa, "Comparison of power spectra for tomosynthesis projections and reconstructed images," *Medical Physics*, vol. 36, no. 5, pp. 1753–1758, 2009.

[14] J. Näppi, P. B. Dean, O. Nevalainen, and S. Toikkanen, "Algorithmic 3D simulation of breast calcifications for digital mammography." *Computer Methods and Programs in Biomedicine*, vol. 66, no. 1, pp. 115–124, Jul. 2001.

[15] J. Ludwig, T. Mertelmeier, H. Kunze, and W. Harer, "A Novel Approach for Filtered Backprojection in Tomosynthesis Based on Filter Kernels Determined by Iterative Reconstruction Techniques," in *LNCS Proceedings of the IWDM*. Springer, 2008, pp. 612–620.

[16] P. R. Bakic, C. Zhang, and A. D. A. Maidment, "Development and characterization of an anthropomorphic breast software phantom based upon region-growing algorithm," *Medical Physics*, vol. 38, no. 6, pp. 3165–3176, 2011.

[17] D. P. Chakraborty and K. S. Berbaum, "Observer studies involving detection and localization: modeling, analysis, and validation." *Medical physics*, vol. 31, no. 8, pp. 2313–2330, Aug. 2004.

[18] D. D. Dorfman, K. S. Berbaum, and C. E. Metz, "Receiver operating characteristic rating analysis. Generalization to the population of readers and patients with the jackknife method." *Investigative radiology*, vol. 27, no. 9, pp. 723–31, Sep. 1992.